AIAA JOURNAL
Vol. 49, No. 8, August 2011

Experimental and Numerical Study of Oscillating Transonic Shock Waves in Ducts

P. J. K. Bruce* and H. Babinsky†
University of Cambridge, Cambridge, England CB2 1PZ, United Kingdom
and
B. Tartinville‡ and C. Hirsch§
NUMECA International, 1170 Brussels, Belgium

DOI: 10.2514/1.J050944

An experimental and computational study of a $M_\infty = 1.4$ transonic shock wave in a parallel-walled duct subject to downstream pressure perturbations in the frequency range of 16–90 Hz has been conducted. The dynamics of unsteady shock motion and aspects of the unsteady transonic shock and turbulent tunnel-floor boundary-layer interaction have been investigated. The numerical computations were performed using an unsteady Reynolds-averaged Navier–Stokes scheme. It is found that the (experimentally measured) shock dynamics are generally well replicated by the numerical scheme, especially at relatively low (≈40 Hz) frequencies. However, variations in shock/boundary-layer interaction structure during unsteady shock motion observed in experiments are not always well predicted by the simulation. Significantly, the computations predict variations in shock/boundary-layer interaction size due to shock motion that are much larger and in the opposite sense to the variations observed in experiments. Comparison of the unsteady results from the present study with steady (experimental) results from the literature suggests that unsteady Reynolds-averaged Navier–Stokes code used in the present study models the unsteady shock/boundary-layer interaction behavior as quasi-steady, whereas experiments suggest that it is more genuinely unsteady. Further work developing numerical methods that demonstrate a more realistic sensitivity of shock/boundary-layer interaction structure to unsteady shock motion is required.

Nomenclature

a	=	local speed of sound, ms^{-1}
C_f	=	skin-friction coefficient
f_{shock}	=	shock-oscillation frequency, Hz
H	=	compressible boundary-layer shape factor, δ^*/θ
H_i	=	incompressible boundary-layer shape factor, δ_i^*/θ_i
M_∞	=	freestream Mach number
p_0	=	tunnel stagnation pressure, kPa
Re_{δ^*}	=	Reynolds number based on boundary-layer displacement thickness, $\rho U_\infty \delta^*/\mu$
St_{inviscid}	=	inviscid Strouhal number for shock-oscillation frequency, $f_{\text{shock}} x_{s-s}/(a-u)$
St_{viscous}	=	viscous Strouhal number for shock-oscillation frequency, $f_{\text{shock}} \delta_0/U_\infty$
U_∞	=	freestream velocity, ms^{-1}
u	=	local flow velocity, ms^{-1}
x, y, z	=	streamwise, tunnel-floor normal, and tunnel spanwise coordinates, mm
x_{s-s}	=	distance between elliptical shaft and mean shock position, mm
δ_0	=	incoming boundary-layer thickness (measured to 99% U_∞), mm
δ^*	=	compressible boundary-layer displacement thickness, $\int_0^\delta (1-(\rho u/\rho_e u_e))\,\mathrm{d}y$, mm
δ_i^*	=	incompressible boundary-layer displacement thickness, $\int_0^\delta (1-(u/u_e))\,\mathrm{d}y$, mm
θ	=	compressible boundary-layer momentum thickness, $\int_0^\delta (\rho u/\rho_e u_e)(1-(u/u_e))\,\mathrm{d}y$, mm
θ_i	=	incompressible boundary-layer momentum thickness, $\int_0^\delta (u/u_e)(1-(u/u_e))\,\mathrm{d}y$, mm

Presented at the 48th AIAA Aerospace Sciences Meeting, Orlando, FL, 4–7 January 2010; received 17 September 2010; revision received 28 February 2011; accepted for publication 1 March 2011.

*Currently Department of Mechanical Engineering, Imperial College London.

†Reader in Aerodynamics, Department of Engineering, Trumpington Street. Associate Fellow AIAA.

‡CFD Group, Chaussée de la Hulpe, 189 Terhulpse Steenweg.

§President, Chaussée de la Hulpe, 189 Terhulpse Steenweg; Professor Emeritus, Vrije Universiteit, Brussels.

I. Introduction

SHOCK/BOUNDARY-LAYER interactions (SBLIs) occur in almost all high-speed aerodynamic applications. Examples include the wings of aircraft traveling at transonic speed, stages of high-speed turbomachinery components, helicopter rotor blades, high-speed ballistics and missiles and the propulsive nozzles and engine intakes of supersonic aircraft. In all of these examples, the behavior of SBLIs is of critical importance for performance and it is for this reason transonic SBLIs are a well-researched and generally well-understood phenomenon. However, all SBLIs are known to exhibit some unsteady behavior and this is one area where our understanding is less comprehensive. This unsteadiness can range from relatively-small-scale fluctuations that produce highly localized effects to more large-scale unsteadiness that can impact an entire flowfield. The large changes in local flow properties that occur through SBLIs mean that unsteadiness can lead to large fluctuations in properties such as pressure and heat transfer, which can lead to undesirable phenomena such as transonic buffeting of aircraft wings, unstarting of supersonic engines, and high levels of unpredictable heat transfer in hypersonic applications. It is primarily a lack of understanding of the mechanisms involved in situations such as these that can make unsteady SBLIs dangerously unpredictable.

Transonic SBLIs are sensitive to both upstream and downstream flow conditions and changes in either can lead to shock motion. The dynamic response of transonic shocks to unsteady pressure perturbations is a complex phenomenon, and our understanding has not reached the level where unsteady shock motion can be predicted reliably. The role and relative importance of inviscid and viscous factors is an area of particular interest and current research [1].

Computational simulations of unsteady compressible internal flows are relatively common [2–4], although the vast majority of these use simplifying assumptions to reduce the complexity of a problem and make it easier to solve. For example, often a flow is assumed to be symmetrical and primarily two-dimensional (or at least quasi-two-dimensional) so that only a section of the real flow is computed (e.g., half or quarter of a channel) and boundary conditions such as sidewalls are simplified by assuming they are inviscid or that the flow is periodic in the spanwise direction. However, the ever-increasing availability of computing power is leading fluid dynamicists to consider the development of new computational approaches and methods for predicted more complex and larger-scale unsteady flows.

A number of experimental and numerical studies [2,3,5–8] have implemented a variable geometry second throat to investigate the effects of downstream periodic pressure perturbations on shocks both experimentally and numerically. The authors of these studies found that the amplitude of shock motion decreased with increasing frequency (see Fig. 1). It was recently shown [9] that the dynamics of normal shocks in simple geometry ducts subject to perturbations in downstream pressure can be predicted analytically and that this analytical relationship could be used to explain the observed amplitude-frequency trend. However, it was found in a related study [10] that transonic shocks exhibited unexpected dynamic behavior as the frequency of downstream pressure perturbations was increased and this was not captured by the analytical model. The reason for this behavior remains an open question, although it has been postulated that viscous effects (such as the mechanism by which downstream disturbances propagate upstream through the flow to reach and influence the shock) may be significant in understanding the physics of unsteady shock motion.

In the present paper, the results from experimental and numerical studies of the response to downstream pressure perturbations of a transonic $M_\infty = 1.4$ shock in a parallel-walled duct are presented. The dynamics of shock motion are analyzed together with the interaction structure between the (naturally grown, tunnel floor) turbulent boundary layer and a transonic shock with and without a fluctuating downstream pressure using modern experimental techniques. Fully three-dimensional, time-accurate numerical simulations are performed using an unsteady Reynolds-averaged Navier–Stokes (URANS) method. Particular attention is given to the comparison of experimental measurements and numerical predictions with an emphasis on understanding the aspects of unsteady SBLIs that a modern URANS code can and cannot yet reliably predict and the reasons behind this. Quantitative analysis of experimentally observed dynamic changes of the unsteady SBLI structure is also carried out to further our understanding of how SBLIs respond in externally unsteady flowfields.

II. Methodology

A. Experiments

Experiments have been performed in the blowdown-type supersonic wind tunnel no. 1 of the University of Cambridge. The tunnel has a rectangular working section with a constant cross section 114 mm wide by 178 mm high. In the present study, the tunnel throat has been set to give a freestream Mach number of 1.4 in the parallel-walled working section. The working section of the tunnel is depicted in Fig. 2a. Downstream of the working section, the flow passes through a 1-m-long diffuser, followed by a long, large, cross-sectional area pipe before entering a large silencing chamber and finally exiting through a series of vents into the atmosphere. The total length of the flow path downstream of the working section is estimated to be 20 m. In the absence of a shock, the streamwise pressure gradient in the parallel-walled tunnel working section is extremely small and streamwise changes in the properties of the naturally grown tunnel-wall boundary layers in the region of interest for this study are negligible. Properties of the incoming boundary layer with this tunnel configuration are presented in Table 1. These measurements are taken at the tunnel centerline.

During unsteady tests, the elliptical shaft seen in Fig. 2a was rotated using a 400 W dc motor mounted outside the tunnel (not shown) at frequencies between 8 and 45 Hz to produce a periodic variation in tunnel backpressure at a frequency double that of shaft rotation. The cycle-averaged variation of downstream pressure measured at transducer T9 ($x = 330$ mm) for the range of cam rotational frequencies tested is plotted in Fig. 2b. The tunnel operating conditions were chosen to give a mean shock position at the center of the viewing window ($x = 0$ mm). Tunnel run times of up to 35 s were possible with the configuration shown in Fig. 2.

High-speed schlieren images of the unsteady flow were captured using a Photron FASTCAM-ultima APX high-speed camera fitted with a 180 mm lens at a frame rate of 4 kHz with an exposure time of 0.125 ms and a resolution of 0.2 mm/pixel. Images presented here have been cropped and processed to remove noise due to irregular camera pixel sensitivity. A line-scanning technique was used to determine the shock position in each frame. The maximum shock speed observed in experiments was 9 ms^{-1}, which implies that the shock could potentially move a streamwise distance of up to 1.1 mm during an exposure. Hence, it is estimated that shock position in a

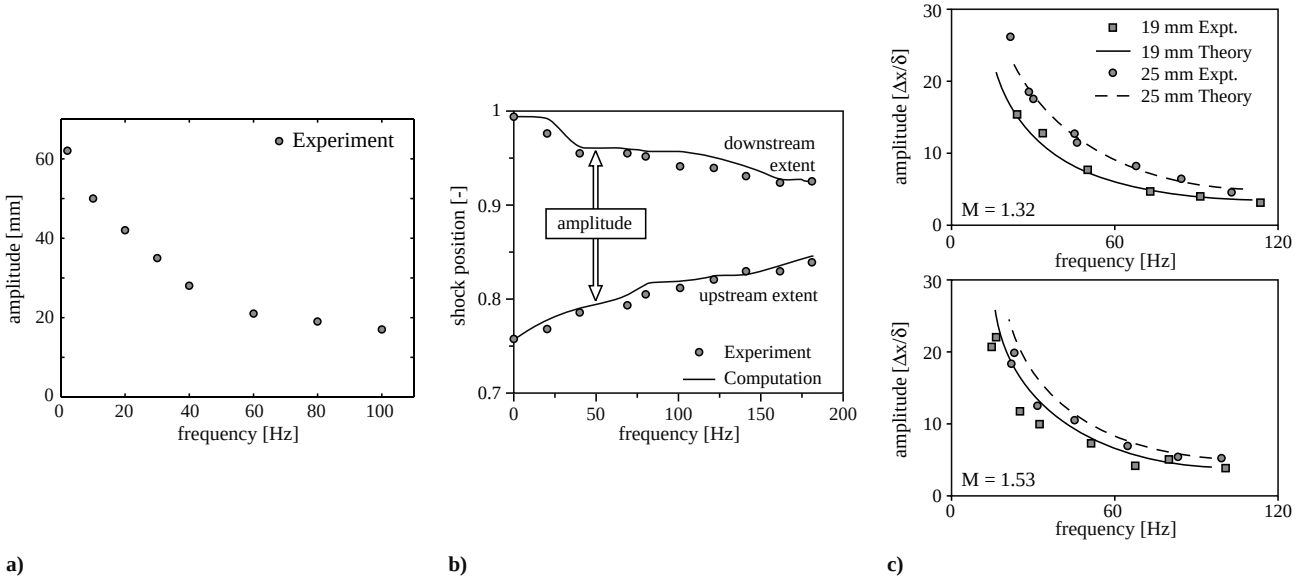

a) b) c)

Fig. 1 Experimental and numerical results showing the relationship between the amplitude and frequency of forced shock motion in a duct from a) Galli et al. [7], b) Ott et al. [2], and c) Edwards and Squire [6].

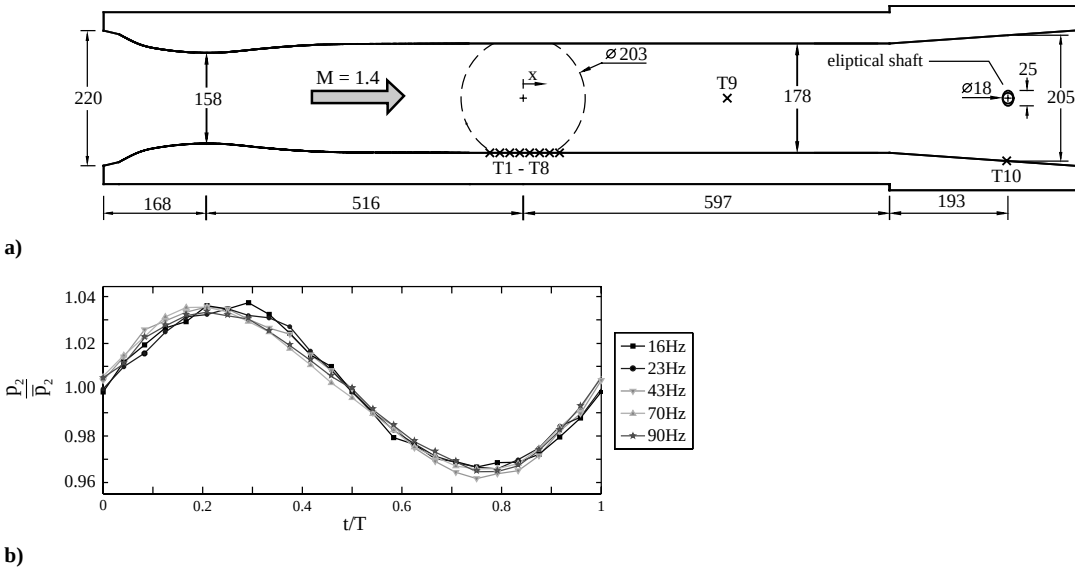

Fig. 2 Experimental arrangement: a) schematic diagram of the working section and b) pressure variation measured at transducer T9. The area of optical access is shown as a dashed circle. The reference location $x = 0$ is defined as the center of this circle. Transducer locations are shown as crosses labeled T1 to T10. All dimensions are in millimeters.

given video frame can be determined with an absolute uncertainty of ± 1 mm (based mainly on shock movement during an exposure) and with an uncertainty relative to its position in a previous or subsequent frame of ± 0.2 mm (based on camera resolution). Based on these values, estimates of shock velocity and acceleration from a single measured cycle of shock motion (calculated with second-order-accurate central-difference schemes based on shock position) have associated uncertainties of approximately ± 0.6 ms^{-1} and ± 2400 ms^{-2}, respectively. To reduce uncertainty in experiments, high-speed video footage of a large number of shock oscillations (typically several hundred) were obtained for each test case and processed to produce a representative average plot of shock position, which was then processed to give information on shock velocity and acceleration. It is estimated that this averaging process reduces the uncertainty in calculated values of velocity and acceleration by at least an order of magnitude relative to the values quoted above for a single cycle.

Static wall-pressure measurements were made using DRUCK PDCR-200 series transducers, labeled T1 to T10 in Fig. 2a. These were calibrated daily and have an accuracy of better than $\pm 1\%$. A sampling rate of 4 kHz was used in both steady and unsteady tests to capture sufficient data for the calculation of reliable mean values. In unsteady tests, pressure data acquisition was synchronized with high-speed schlieren video to allow the pressure data to be sorted temporally and spatially relative to the instantaneous position of the shock wave in the tunnel. Pressure data obtained this way in the region of the shock wave (sampled at transducers T1–T8) were then processed using a rolling-average technique with a bin size of 6 mm to produce the plots presented in this paper.

Table 1 Characteristic parameters of the incoming boundary layer in experiments

Parameter	Value[a]
P_0, kPa	140
M_∞	1.4
δ, mm	4.6
δ^*, mm	0.56 (0.80)
θ, mm	0.41 (0.37)
H_i	1.35 (2.15)
Re_{δ^*}	(18,500)
C_f	0.00214

[a]Incompressible values are given, with compressible values in parentheses.

Velocity measurements of the unsteady flowfield have been made using laser Doppler anemometry (LDA). The measuring volume diameter was approximately 75 μm and measurements were possible 0.1 mm away from the wall. Olive oil droplets with mean diameter of 200 nm were used to seed the flow, and data rates in excess of 50 kHz were realized. Despite this high data rate, a large number of tunnel runs were required to fully characterize the unsteady flowfield. Data processing of LDA measurements involved using high-speed schlieren images to determine the precise location of the LDA measurement volume at all times relative spatially to the shock and also temporally within the cycle of shock motion. The measuring volume position was then changed between runs to gradually build up a complete picture of the flow at different points in the cycle. For a more detailed description of the experimental facility and methodology, the reader is referred to previously published work [9,11].

B. Numerical Simulations

Numerical simulations of the steady and unsteady flowfields have been performed by NUMECA International using their FINE/Turbo flow solver [12]. The flow solver is a three-dimensional, explicit, density-based, structured, multiblock URANS code using the finite volume approach. Central-space discretization is employed together with Jameson-type artificial dissipation. A four-stage Runge–Kutta scheme is selected for the temporal discretization. Multigrid, local time-stepping, and implicit residual smoothing are also used in order to speed up the convergence. Time-accurate computations (that allow the unsteady viscous aspects of the flow to be resolved) are done with a dual-time-stepping method. The temporal derivative is discretized using a second-order backward Euler difference. In an effort to capture the experimental inflow as accurately as possible, simulations have modeled the tunnel upstream of the working section. A typical computational mesh is shown in Fig. 3. Results presented here have been obtained using the two-equation k-ϵ turbulence model developed by Yang and Shih [13]. Further details of the numerical method and grid can be found in a previously published paper [14].

To simulate the downstream pressure disturbances generated at the rotating elliptical shaft in experiments, time-accurate simulations of the complete tunnel working section with a rotating mesh at the shaft have been performed. The temporal resolution was chosen to give 160 time steps per revolution of the shaft. The results of these simulations are presented in Fig. 4. Figure 4b shows that the pressure waves generated at the elliptical shaft rapidly develop into highly

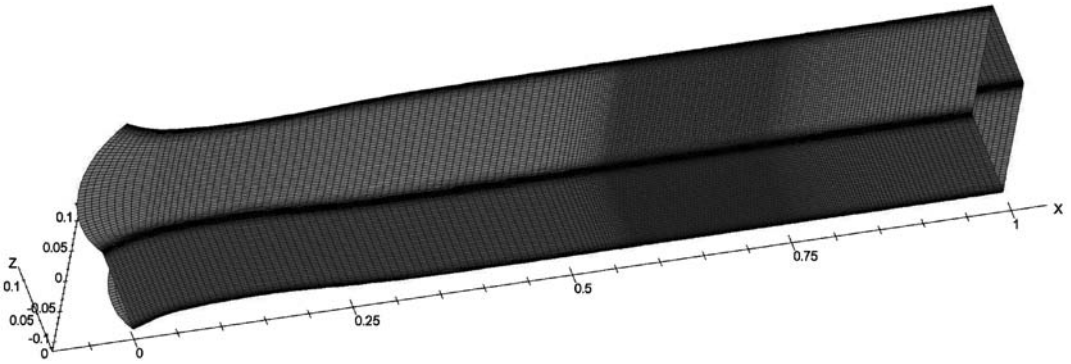

Fig. 3 Typical computational mesh used for steady and unsteady calculations (3,300,000 cells).

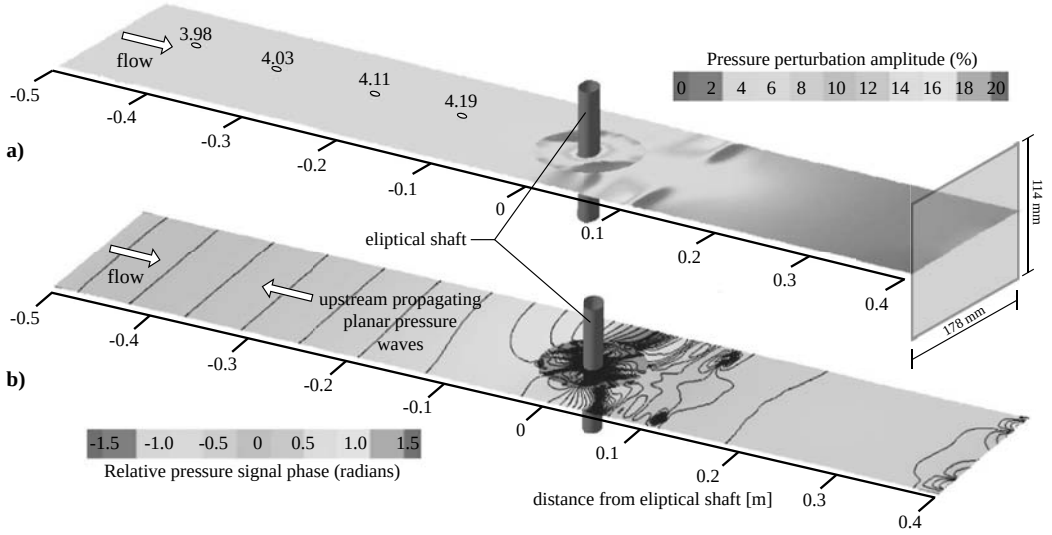

Fig. 4 Simulated pressure waves generated at the elliptical shaft: a) pressure disturbance amplitude and b) pressure disturbance phase. The shaft rotational frequency is 20 Hz, which produces a 40 Hz pressure perturbation.

planar waves as they travel upstream. Figure 4a shows that the strength of these waves remains almost constant as they travel upstream with an amplitude of around 4% of the mean local static pressure (as annotated at four points upstream of the shaft on the plot). For reference, the downstream pressure in experiments is measured 0.46 m upstream of the shaft (transducer T9, see Fig. 2) and the shock is located 0.79 m (on average) upstream of the shaft.

III. Results

A. Characterization of the Steady $M_\infty = 1.4$ SBLI

Experimental and numerical results that characterize the steady $M_\infty = 1.4$ SBLI are presented in Fig. 5. In these tests, the elliptical shaft shown in Fig. 2a was held stationary to impose a constant backpressure. High-speed schlieren video of the so-called steady shock wave in experiments with this arrangement revealed that the shock position remained constant to within ± 1 mm during steady tests. The schlieren photograph from experiments in Fig. 5a shows the existence of a λ shock foot with a faint leading shock leg. This suggests that the interaction is somewhere in-between the classical weak (attached) and strong (separated) cases that are well documented in the literature [15,16]. The surface oil-flow visualization from experiments in Fig. 5c shows no evidence of reversed (separated) flow, although a large decrease in surface shear stress at the shock location does exist (see annotation). There is evidence that significant regions of the flow are affected by the presence of the tunnel corners. The experimentally measured static pressure rise through the interaction in Fig. 5e is consistent with that for an attached interaction (see, for example, [15]).

The velocity profiles in Fig. 5f show that the inflow upstream of the interaction is well predicted by the numerical scheme, although the boundary layer is slightly too thick ($\delta \approx 6$ mm compared with 4.6 mm in experiments). Downstream of the interaction, the agreement is less good: the numerical scheme appears to overpredict the rate at which the postshock boundary layer recovers, and this leads to a boundary layer that has too full of a profile in the near-wall region. The postshock freestream velocity is also overpredicted slightly. A possible explanation for this is that the large interaction sizes predicted by the numerical scheme (especially in the corners and on the sidewalls) cause more of a blockage effect for the core flow, which leads to a greater centerline acceleration.

Overall, the numerical results presented in Fig. 5 show a reasonable level of agreement with experiments, although some discrepancies exist. The most significant discrepancy is an overprediction of the interaction size. This leads to a larger, more smeared, interaction structure than was observed in experiments (compare Figs. 5a and 5b) and also to an overestimate of the predicted interaction upstream influence, which can be seen clearly in the plot of static pressure (Fig. 5e). The surface streamlines predicted by the numerical solution (Fig. 5d) show that the size of the corner effects are also slightly overpredicted, which indicates that the SBLIs on the tunnel sidewalls are also slightly too large.

No asymmetry was observed in any of the steady or unsteady experimental or numerical results presented here. Although the flow does exhibit some three-dimensionality, these three-dimensional aspects are seen in both experimental and computational results. This gives some confidence in the numerical scheme's ability to capture such features of the flow, and hence these features are not considered

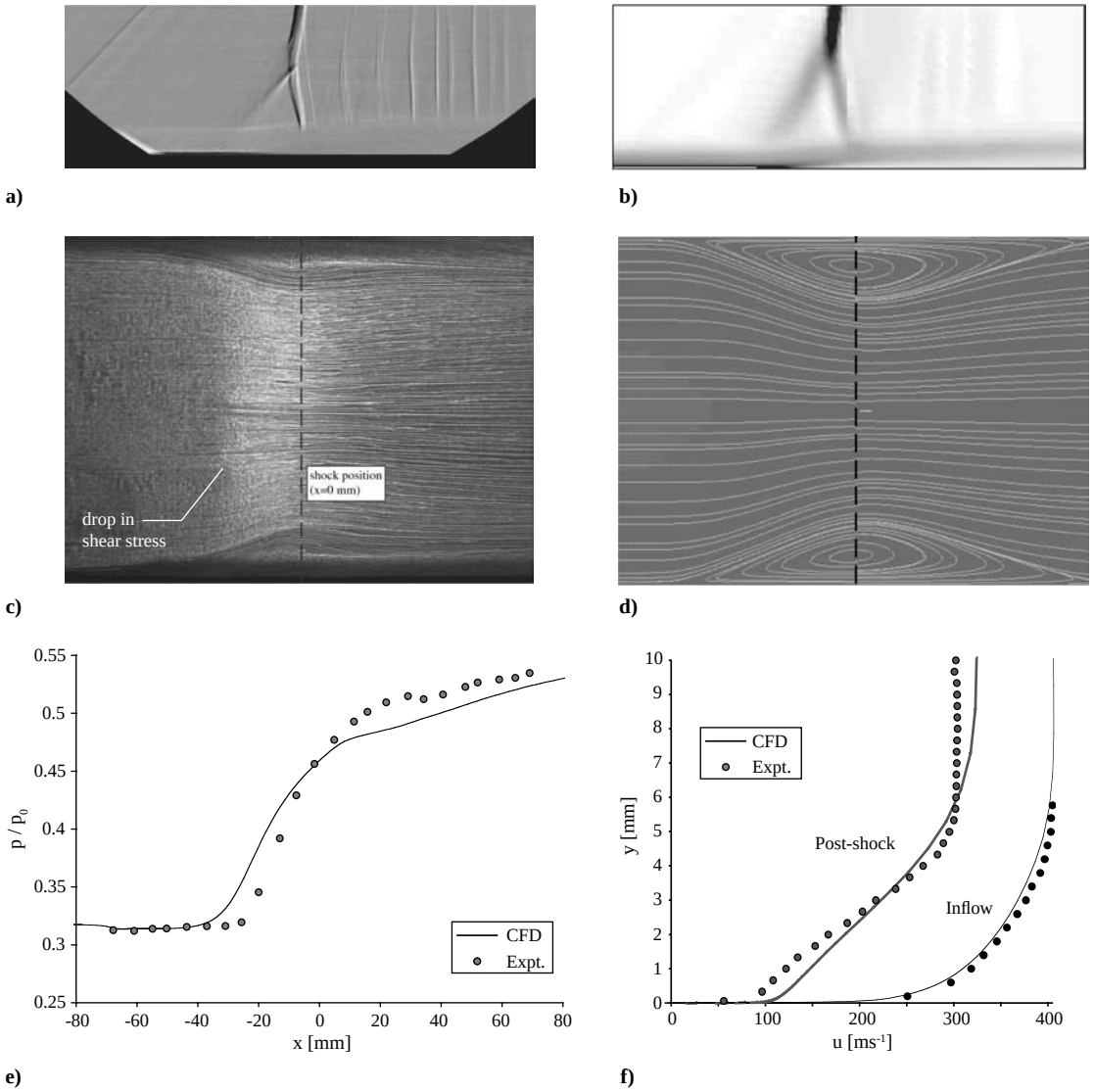

Fig. 5 Steady $M_\infty = 1.4$ SBLI: a) schlieren image from experiment, b) numerical schlieren, c) surface oil-flow visualization, d) numerically predicted surface streamlines, e) surface pressure distribution, and f) boundary-layer profiles. The surface pressure data from experiments are time-averaged

to prevent a valuable comparison between the experimentally measured and numerically simulated flowfields.

B. Shock Dynamics of a $M_\infty = 1.4$ SBLI Subject to Unsteady Forcing

In the absence of an imposed downstream pressure variation, the transonic $M_\infty = 1.4$ shock exhibited no large-scale self-excited unsteady motion. When subjected to sinusoidal variations of downstream pressure, the tunnel's normal recovery shock was observed to undergo periodic oscillatory motion in the streamwise direction. Experiments with forced shock-oscillation frequencies of 16, 23, 43, 70, and 90 Hz were performed. These frequencies are compared with two relevant timescales of the flow through the calculation of two different Strouhal numbers: First, a so-called viscous Strouhal number is defined as

$$St_{\text{viscous}} = f_{\text{shock}}\delta_0/U_\infty \tag{1}$$

where f_{shock} is the frequency of forced shock oscillation, U_∞ is the incoming freestream velocity (=410 ms^{-1}) and δ_0 is the incoming boundary-layer thickness (=4.6 mm). Second, an inviscid Strouhal number is defined as

$$St_{\text{inviscid}} = f_{\text{shock}}x_{s-s}/(a-u) \tag{2}$$

where $(a-u)$ is the acoustic wave speed downstream of the shock ($\approx$50 ms^{-1}) and x_{s-s} is the mean streamwise distance between the elliptical shaft and the shock wave (=790 mm).

Using the above definitions, the frequencies investigated in the present study yield values of $0.00018 < St_{\text{viscous}} < 0.00101$ and $0.25 < St_{\text{inviscid}} < 1.42$. These results show that the shock wave excitation frequencies are very low compared with characteristic viscous timescales of the flow, but they are comparable with the inviscid (acoustic) timescales. This suggests that the shock wave's response to periodic forcing is likely to be acoustically driven and that viscous aspects of the flow (such as SBLIs) are likely to behave in a quasi-steady manner.

Schlieren images showing four points in a single period of shock oscillation with a forcing frequency of 43 Hz are shown in Fig. 6. Points A and C correspond to when the shock is at its most downstream and upstream positions during an oscillation, respectively. Points B and D correspond to when the shock is at the mean position in its oscillation ($x = 0$ mm) and is traveling upstream and downstream, respectively.

It has been shown that the dynamics of shock motion are related primarily to changes in the relative Mach number ahead of the shock that occur as the shock moves [9]. Furthermore, it was also shown that these changes in relative Mach number are determined by the imposed pressure ratio across the interaction. Specifically, an imposed rise in backpressure increases the pressure ratio across the

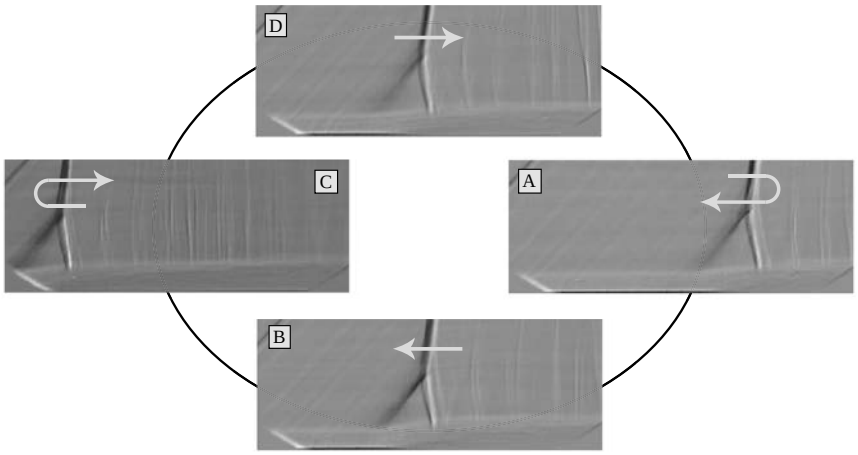

Fig. 6 Schlieren images of the unsteady SBLI; $M_\infty = 1.4$ and frequency is 43 Hz. The white arrows on the images indicate the direction (or a change in direction) of shock motion.

shock, which causes the shock to move upstream in the parallel-walled duct in order to increase its relative strength and satisfy the imposed pressure ratio. The experimentally measured pressure rise through the unsteady interaction during upstream and downstream shock motions is plotted in Fig. 7 together with the pressure profiles predicted by the unsteady numerical simulation at the corresponding points in the cycle of shock motion.

Figure 7 shows reasonable agreement between the experimentally measured pressure rises through the unsteady interaction and those predicted by the numerical scheme. The agreement for downstream shock motion is better than for upstream shock motion. In the latter case, the numerical simulation overpredicts the upstream influence of the interaction and does not capture the shape of the pressure rise observed in experiments, especially around $x = 20$ mm, where a kink is present in the pressure distribution that is not seen in experiments.

The magnitude of the pressure rise through the unsteady interaction is reasonably well predicted by the numerical scheme for both upstream and downstream shock motions. This suggests that the simulation is correctly modeling the downstream conditions imposed on the shock in experiments. In light of this, the relationship between imposed pressure ratio and shock dynamics previously proposed by Bruce and Babinsky [9] suggests that an unsteady computational code should be able to reproduce the shock dynamics observed in experiments. To investigate this, the experimentally measured and numerically predicted dynamics of forced shock motion at two frequencies are analyzed in Figs. 8 and 9. The amplitude of shock oscillation (plotted in Fig. 8c and discussed subsequently in this paper) is defined as the difference between the most upstream and downstream shock positions observed at midheight in the tunnel ($y = 89$ mm) in the plots of average shock position obtained for each test case.

Figure 8a shows that both the amplitude and peak acceleration of shock motion vary considerably with shock-oscillation frequency. In contrast, variations in shock velocity are small, with the exception of the high-frequency (70 and 90 Hz) test cases, where some notable "wiggles" in velocity begin to appear near the start of the cycle ($0 \leq t/T \leq 0.3$). Figure 8c shows that the numerically predicted values of shock-oscillation amplitude closely match those from experiments and are in agreement with the experimentally observed trend of decreasing oscillation amplitude with increasing frequency.

Figure 9a shows good agreement between the experimentally measured and numerically predicted shock velocity profiles for a shock-oscillation frequency of around 40 Hz, although the numerical scheme slightly overpredicts peak shock velocities. In contrast, the agreement for the 90 Hz test case (Fig. 9b) is significantly worse. Here, the numerical scheme overpredicts the peak downstream (positive) shock velocity observed in experiments by around 50% and does not replicate the experimentally observed shape of the velocity profile. It should be noted, however, that the numerically

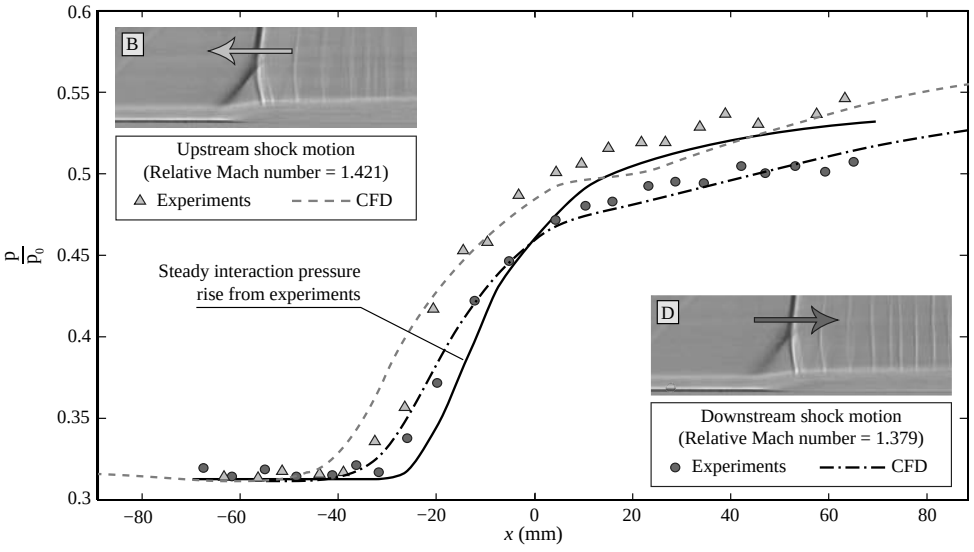

Fig. 7 Comparison of the static pressure rise through a $M_\infty = 1.4$ SBLI during upstream and downstream motion. The oscillation frequency is 43 Hz in the experiment and 40 Hz in the numerical simulation.

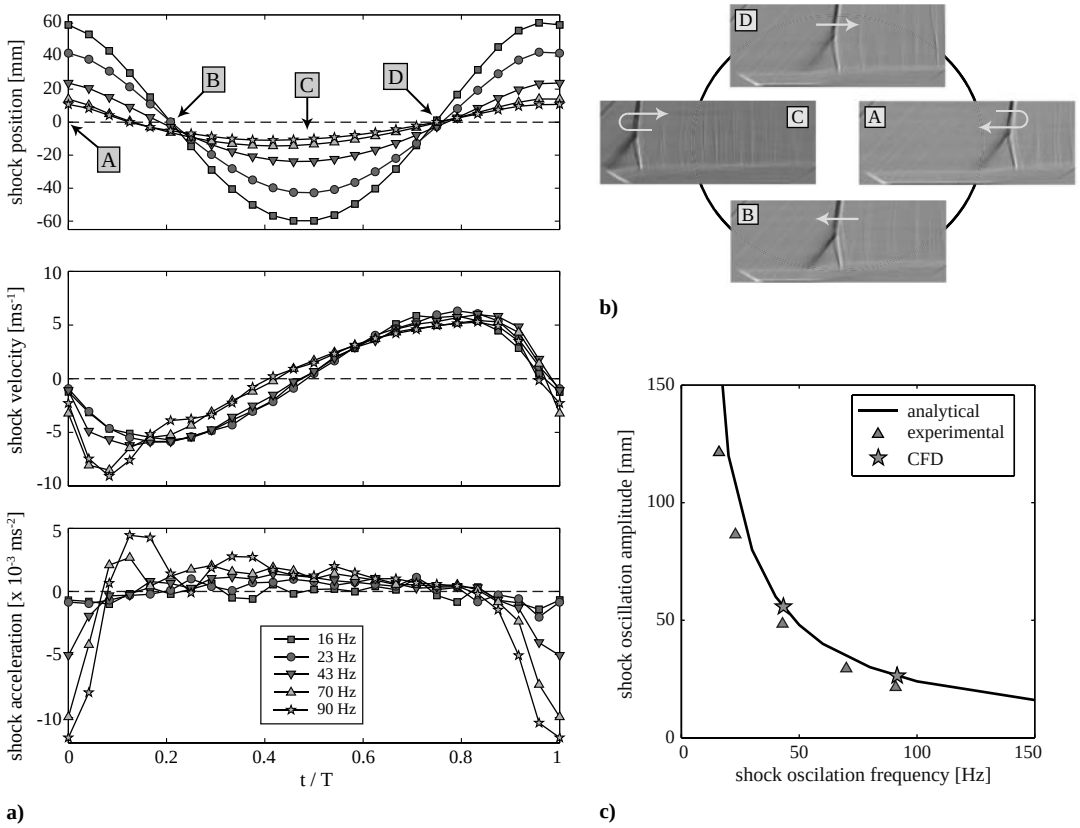

Fig. 8 Experimentally measured dynamics of unsteady shock motion at $M_\infty = 1.4$: a) shock dynamics (positive values are downstream), b) schlieren images, and c) amplitude/frequency relationship. The analytical solution is taken from Bruce and Babinsky [9].

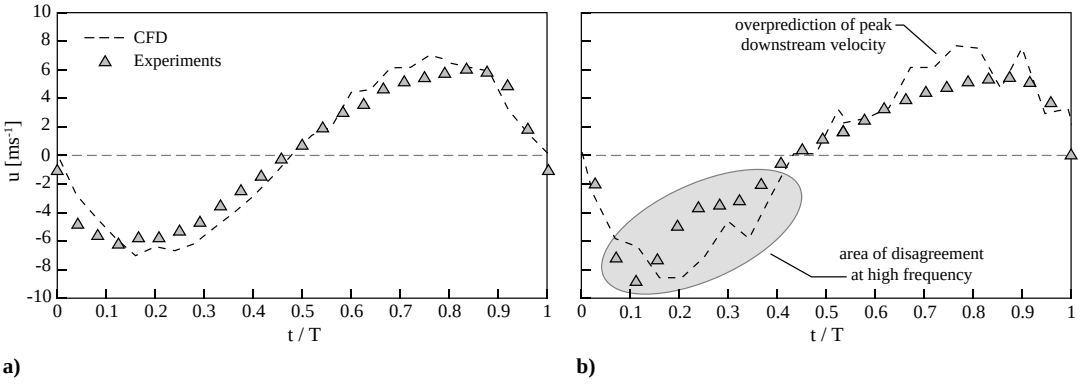

Fig. 9 Comparison of numerically predicted and experimentally measured shock dynamics at $M_\infty = 1.4$: a) 40/43 Hz (simulation/experiment) and b) 90 Hz.

predicted velocity data for the 90 Hz test case appear to be quite noisy and so no firm conclusions should be drawn.

Figures 8 and 9 show that the numerical scheme used in this study is generally capable of replicating the experimentally measured dynamics of shock motion in response to an imposed downstream pressure variation, although some discrepancies seem to exist as frequency is increased. It is possible that the success of the numerical scheme in this area stems from the fact that the main aspects of shock motion are governed by inviscid effects (almost one-dimensional upstream-traveling pressure waves), which are relatively well understood and captured by the numerical URANS code. Thus, the success of the numerical scheme in capturing the viscous nature of the unsteady SBLI is yet to be been determined. To address this unanswered question, the (numerically predicted and experimentally measured) viscous SBLI structure during forced unsteady shock motion is examined next.

C. Changing Viscous Interaction Structure of an Unsteady SBLI

Schlieren images from experiments showing the four points A–D in individual shock oscillations at three different forcing frequencies are shown in Fig. 10.

The images in Fig. 10 show that changes to the interaction structure due to shock motion are relatively subtle for each individual test case (compare images A, B, C, and D) and also between different frequency test cases (compare images at 23, 43, and 90 Hz). The interaction size increases slightly when the shock is downstream (image A) and the leading leg of the λ shock-foot structure appears more well-defined during upstream shock motion (image B) than it is during downstream shock motion (D). This difference in appearance can be explained by changes in the strength of the leading leg of the λ shock structure as the relative Mach number of the incoming flow varies as the shock moves. Specifically, as the shock moves upstream, the relative Mach number increases and the leading leg

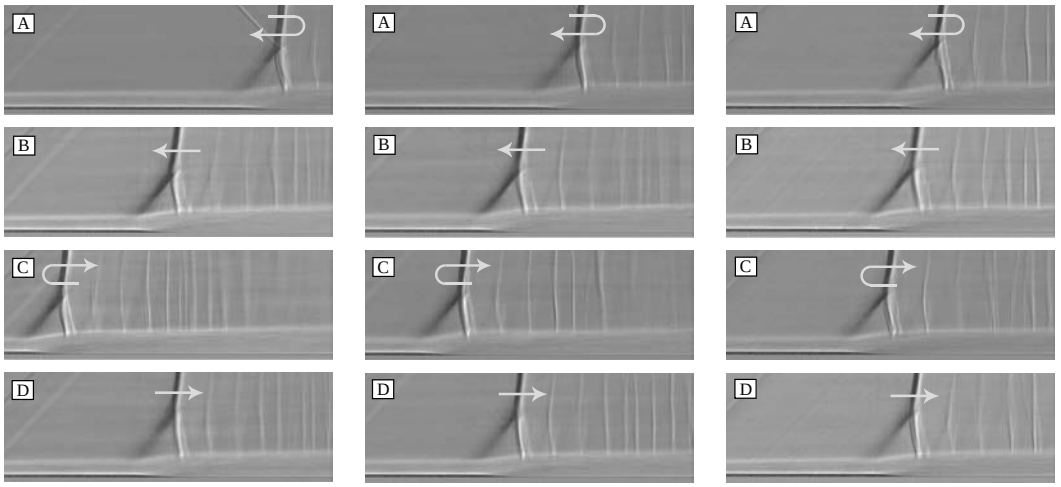

Fig. 10 Schlieren images from experiments at different frequencies with $M_\infty = 1.4$: a) $f_{shock} = 23$ Hz, b) $f_{shock} = 43$ Hz, and c) $f_{shock} = 90$ Hz.

gets stronger to accommodate the increased pressure jump through the shock. The measured pressure profiles in Fig. 7 show that the initial pressure rise through the unsteady interaction is steeper when the shock moves upstream, which supports the idea that the leading leg of the λ shock structure should be stronger.

The images in Fig. 10 also show that a number of well-defined but relatively weak secondary shock waves or wavelets can be seen downstream of the main shock wave. Careful analysis of high-speed video frames reveals that these wavelets propagate upstream toward the shock wave. It is thought that they are formed when the compressive pressure waves produced by the elliptical shaft coalesce as they propagate slowly upstream in the high-subsonic Mach number postshock flow to become weak upstream-traveling shock waves (or wavelets). The pattern of these wavelets varies during the cycle of shock motion but is similar at different frequencies. Figure 11 shows equivalent numerical schlieren plots of the unsteady SBLI during upstream and downstream shock motions.

Figure 11 shows that the numerical scheme generally predicts interaction sizes that are much greater than those observed in experiments, in agreement with the trend observed for the steady case (Fig. 5). It can also be seen in Fig. 11 that the numerical scheme predicts a much greater variation in interaction size between upstream and downstream shock motions than is observed in experiments. It is not clear from Fig. 11b whether the leading leg of the λ shock-foot structure in the numerical solution varies in intensity during upstream and downstream motion, as was observed to be the case in experiments. However, it is interesting to note that the numerically predicted pressure profiles in Fig. 7 show that the initial pressure rise in both cases are rather similar, more so than in experiments.

To quantitatively investigate the observed variation in experimentally measured and numerically predicted interaction size, the position of the triple point (at the top of the λ shock foot, as annotated in Fig. 11) has been tracked during unsteady shock motion. The results from this are presented in Fig. 12.

Figure 12a confirms that the triple-point height (which is a measure of the interaction size) predicted by the numerical scheme is, on average, larger than in experiments by around 40%. In addition, a

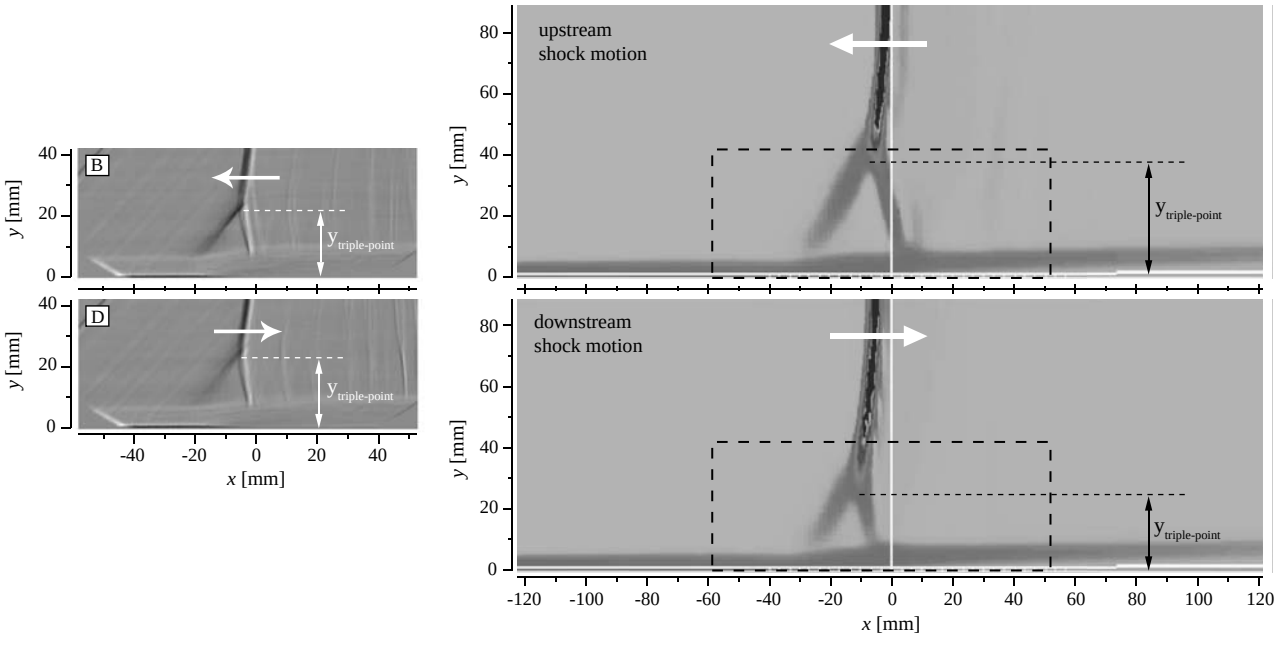

Fig. 11 Comparison of the interaction structure predicted by the numerical scheme for upstream and downstream shock motions: a) schlieren images from experiment with $f_{shock} = 43$ Hz and b) numerical schlieren images with $f_{shock} = 40$ Hz. Both plots are shown at the same scale. Numerical schlieren images show the bottom half of the tunnel ($0 < y < 89$ mm) only.

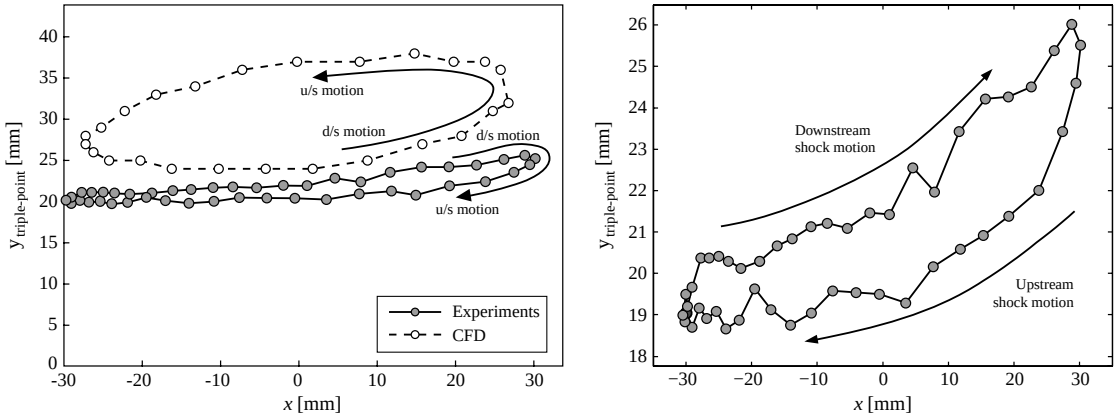

a) b)

Fig. 12 Evolution of triple-point height during unsteady shock motion: a) comparison of experimental (43 Hz) and numerical (40 Hz) results and b) zoom of experimental results.

number of other discrepancies between experimental and numerical results exist. Parameters that highlight these differences are summarized in Table 2. First, the variation in triple-point height due to shock motion is overpredicted (10–15 mm difference between upstream/downstream shock motion compared with 2–3 mm difference in experiments). Second, the numerical scheme predicts that the triple point should be larger during upstream shock motion than during downstream shock motion, whereas the opposite trend is observed in experiments. Interestingly, these two discrepancies lead to the numerical scheme predicting that the maximum interaction size should occur during upstream shock motion, whereas experiments suggest that the maximum occurs when the shock is in its most downstream (positive) position and is stationary.

Figure 12 shows that a hysteresis in triple-point height between upstream and downstream shock motions occurs in both the numerical simulation and the experiment. Both curves show a trend for the triple-point height to increase with downstream position by around 30% of its value at its most upstream position (Fig. 12b shows this most clearly for the experimental results). This increase is attributed in part to the natural streamwise growth of the tunnel-floor boundary layer that would occur over the streamwise distance of shock motion ($\approx$60 mm) even if the shock wave was not present. However, measurements of the tunnel-floor boundary layer in the working section (when there is not a shock wave and the flow is supersonic) have shown that the boundary layer grows at an approximately linear rate of 0.8 mm per 100 mm streamwise distance, which would correspond to an increase in δ of less than 0.5 mm (around 10%) over a 60 mm streamwise distance. It is reasonable to assume that this would cause an increase in triple-point height of around 10%, which is significantly lower than the 30% difference observed in experiments. Hence, it is likely that there are other contributory factors that cause the triple-point height to increase with downstream shock position.

Figure 12a also suggests that there is a small difference in the experimentally measured and numerically predicted amplitudes of shock oscillation, which is in apparent disagreement with Fig. 8c. However, this difference is thought to be caused by slight differences in the amount of (wall-normal) shock curvature that occur at different phases of the unsteady shock's motion (i.e., the position of the shock at the tunnel centerline varies slightly relative to the streamwise position of the triple point). Hence, it may be possible that the numerical scheme predicts the correct amplitude of shock motion at the tunnel centerline and not at the location of the triple point. Another possibility is that the large change in height of the triple point seen in numerical results has an effect on its streamwise position (as the shock is slightly inclined and also curved close to the floor).

In summary, the parameters in Table 2 suggest that the numerical scheme does not fully capture the dominant mechanisms (which may be viscous) that are responsible for the changes in interaction structure observed in experiments. In particular, the different interaction size during upstream and downstream shock motions seen in experiments and in the numerically predicted flow is an area of significant disagreement. Previous studies have shown that the interaction size, and hence triple-point height, of a steady transonic SBLI should increase as the Mach number ahead of the shock is increased [17]. This trend is illustrated by the data plotted in Fig. 13, which are taken from steady tests at a range of Mach and Reynolds numbers.

Experimental and numerical results from the present study have been plotted in Fig. 13b. These data points correspond to the steady interaction and also the points during unsteady upstream and downstream shock motions when the shock is at $x = 0$ mm (points B and D in previous figures). These data points have been chosen to attempt to isolate the effects of shock motion. For the unsteady test cases, the measured triple-point height (normalized by the incoming boundary-layer thickness) is plotted against the *relative* Mach number ahead of the shock wave, calculated using the measured shock velocities in Fig. 9.

The difference between the steady experimental and numerical data points from the present study in Fig. 13b emphasizes the fact that the numerical scheme overpredicts steady interaction size, whereas (encouragingly) the experimental result from the present study shows excellent agreement with the experimental data of Doerffer

Table 2 Comparison of unsteady interaction parameters from experiment and numerical simulation

Parameter	Experiment	Simulation
Frequency, Hz	43	40
Oscillation amplitude at tunnel centerline, mm	48	62
Oscillation amplitude at triple point, mm	60	54
Mean triple-point height, mm	22	31
Minimum/maximum triple-point height, mm	19/26	24/38
Variation in triple-point height due to motion, mm	2–3	10–15
Triple point higher during...	Downstream motion	Upstream motion

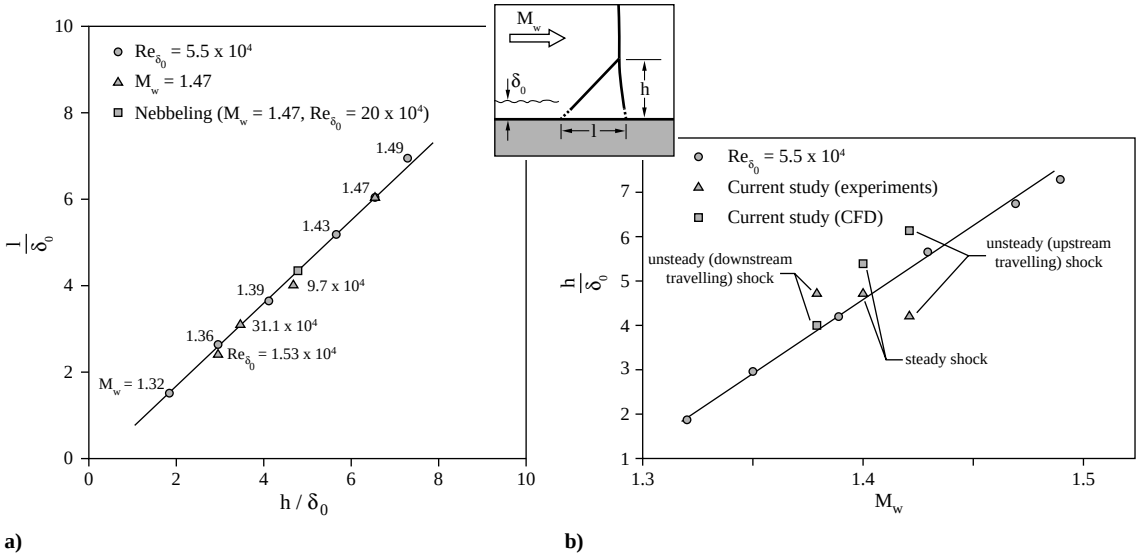

Fig. 13 Variation of steady transonic SBLI geometry with Mach number: a) bifurcation topography and b) effect of Mach number on bifurcation (triple-point) height. The parameters l, h, δ_0, and M_w used in the plots are defined in the (inset) schematic diagram. Figures are adapted from Doerffer [17].

[17]. However, data points from unsteady experiments do not lie on the trend line and do, in fact, show a correlation in the opposite sense (i.e., interaction size decreases with increasing relative shock strength). In contrast, the unsteady numerical results in Fig. 13b show the same trend as the steady experimental data from Doerffer (i.e., increasing interaction size with increasing shock strength), albeit with a slightly greater gradient. This suggests that the changes in interaction structure predicted by the numerical scheme are primarily related to variations in relative shock strength and these changes would be more-or-less correct if the interaction behaved in a truly quasi-steady manner (although the larger gradient observed for the numerical results would suggest that the sensitivity of interaction size to shock strength is being overpredicted).

However, this explanation is contradicted by the results from unsteady experiments, which suggest that the unsteady transonic SBLI does not behave quasi-steadily, and that other factors that affect the interaction size must also be important. In addition to the results at points B and D from unsteady experiments that are plotted in Fig. 13b, the unsteady SBLI structure also exhibits what could be referred to as non-quasi-steady behavior at points A and C in its cycle. In these cases (where the shock wave is momentarily stationary at the extreme positions of its motion) even though the relative Mach number of the shock is the same (and equal to the freestream value of 1.4), the ratio of interaction size to boundary-layer thickness is not constant, which would be the expected result if the flow behavior was truly quasi-steady.

Experimentally measured and numerically predicted Mach number contours at the tunnel centerline during upstream and downstream shock motions are plotted in Fig. 14.

Figure 14 emphasizes the fact that the numerical scheme overpredicts interaction size and the magnitude of changes in interaction size due to shock motion. However, the velocity contours in Fig. 14 also show some similarities between the unsteady SBLI observed in experiments and predicted by the numerical simulation. First, the Mach number downstream of the SBLI is lower when the shock is traveling upstream, and second, boundary-layer growth through the interaction is larger during upstream than downstream shock motion. This suggests that even though the boundary layer appears to feel and respond to the variations in adverse pressure gradient that occur in experiments (due to shock motion), the size of

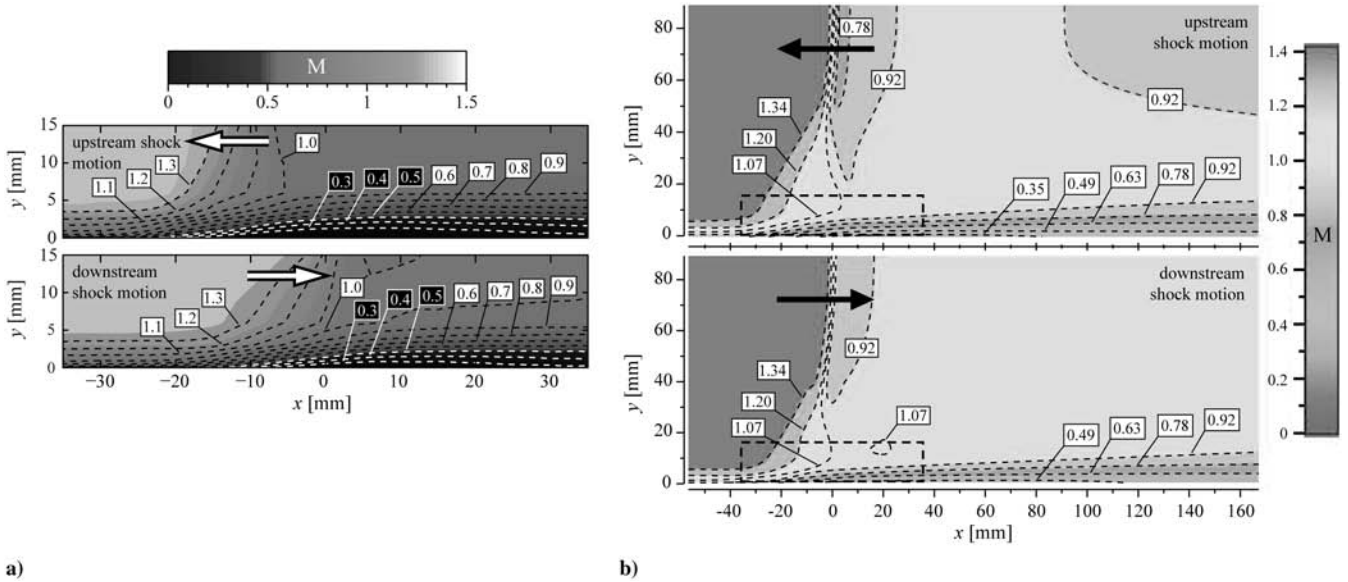

Fig. 14 Mach number contours for upstream and downstream shock motions from a) experiments and b) numerical simulation. Plots are shown at different scales and have different shaded scales and contour levels.

the λ shock foot does not match the quasi-steady expectation (that it should get larger as the shock moves upstream and smaller when the shock moves downstream).

As discussed previously, the viscous timescales of the flow are much shorter than the period of shock motion ($St_{\text{viscous}} \ll 1$). In contrast, the acoustic timescales of the flow are much closer to the period of shock motion ($St_{\text{inviscid}} \approx 1$). Based on this, it can be speculated that the non-quasi-steady variation of SBLI size may stem from the existence of some sort of phase lag between the arrival time of downstream pressure information in inviscid regions of the flow (such as downstream of the main shock and behind the λ shock structure) and in viscous regions (such as the floor and sidewall boundary layers and any corner flows). To explore this possible mechanism, further research in this area is required, ideally including both further detailed experiments and the development of improved numerical methods for simulating aspects of unsteady transonic flows.

IV. Conclusions

Experimental and computational studies of a $M_\infty = 1.4$ transonic shock/boundary-layer interaction (SBLI) in a duct with parallel walls with and without downstream pressure perturbations have been performed. In the absence of pressure perturbations (steady test case), it is found that the numerical method overestimates interaction size but is otherwise largely successful in predicting most features of the SBLI. When low-frequency (40 Hz) downstream pressure perturbations are introduced, the numerical scheme predicts realistic shock motion but fails to replicate the subtle changes in the viscous SBLI structure that are observed in experiments. The changes due to shock motion predicted by the numerical scheme are consistent with what would be expected if the unsteady flow could be treated as quasi-steady (specifically, that the interaction structure should be determined solely by the relative shock strength, which varies due to shock motion). However, the variations in the size of the SBLI structure observed in unsteady experiments suggest that this is not the case and that the interaction is, in fact, influenced by more complex effects. It is speculated that some sort of phase lag may exist between the behavior of the λ shock structure and the boundary layer, due to the different inviscid and viscous timescales present in the flow.

At higher frequencies (90 Hz), the numerical scheme fails to replicate aspects of the experimentally observed shock dynamics (which were different from those at low frequency). This supports the theory that the numerical method used in the present study did not completely capture all of the relevant unsteady flow physics for the unsteady SBLI observed in experiments (which in itself cannot yet necessarily be explained). Further work developing numerical methods that accurately model the sensitivity of the SBLI structure to shock motion at a range of frequencies is desirable. Improvements in this area are likely to result in improvements to methods for modeling SBLIs with and without artificial unsteadiness (as all SBLIs are known to exhibit some unsteady behavior). Further experimental work examining the dynamics of shock behavior at frequencies above 90 Hz would also be beneficial for increasing our understanding of the unsteady (possibly viscous) mechanisms at work.

Acknowledgment

The present collaborative research was funded under the European Union Framework 6 programme UFAST.

References

[1] Doerffer, P., Hirsch, C., Dussauge, J.-P., and Babinsky, H. (eds.), *Unsteady Effects of Shock Wave Induced Separation: 220*, Notes on Numerical Fluid Mechanics and Multidisciplinary Design, 1st ed., Springer, New York, 2010.

[2] Ott, P., Bolcs, A., and Fransson, T. H., "Experimental and Numerical Study of the Time-Dependent Pressure Response of a Shock Wave Oscillating in a Nozzle," *Journal of Turbomachinery*, Vol. 117, 1995, pp. 106–114. doi:10.1115/1.2835625

[3] Handa, T., Masuada, M., and Matsuo, K., "Mechanism of Shock Wave Oscillation in Transonic Diffusers," *AIAA Journal*, Vol. 41, No. 1, 2003, pp. 64–70. doi:10.2514/2.1914

[4] MacMartin, D. G., "Dynamics and Control of Shock Motion in a Near-Isentropic Inlet," *Journal of Aircraft*, Vol. 41, No. 4, 2004, pp. 846–853. doi:10.2514/1.416

[5] Sajben, M., Bogar, T. J., and Kroutil, J. C., "Forced Oscillation Experiments in Supercritical Diffuser Flows," *AIAA Journal*, Vol. 22, 1984, pp. 465–474. doi:10.2514/3.8423

[6] Edwards, J. A., and Squire, L. C., "An Experimental Study of the Interaction of an Unsteady Shock with a Turbulent Boundary Layer," *The Aeronautical Journal*, Vol. 97, No. 970, 1993, pp. 337–348.

[7] Galli, A., Corbel, B., and Bur, R., "Control of Forced Shock-Wave Oscillations and Separated Boundary Layer Interaction," *Aerospace Science and Technology*, Vol. 9, 2005, pp. 653–660. doi:10.1016/j.ast.2005.07.008

[8] Bur, R., Benay, R., and Galli, A., and Berthouze, P., "Experimental and Numerical Study of Forced Shock-Wave Oscillations in a Transonic Channel," *Aerospace Science and Technology*, Vol. 10, 2006, pp. 265–278. doi:10.1016/j.ast.2005.12.002

[9] Bruce, P. J. K., and Babinsky, H., "Unsteady Shock Wave Dynamics," *Journal of Fluid Mechanics*, Vol. 603, 2008, pp. 463–473. doi:10.1017/S0022112008001195

[10] Bruce, P. J. K., and Babinsky, H., "Unsteady Normal Shock Wave Boundary Layer Interactions with Control," AIAA Paper 2008-0721, 2008.

[11] Bruce, P. J. K., and Babinsky, H., "An Experimental Study of Transonic Shock/Boundary Layer Interactions Subject to Downstream Pressure Perturbations," *Journal of Aerospace Science and Technology*, Vol. 14, No. 2, March 2010, pp. 134–142. doi:10.1016/j.ast.2009.11.006

[12] "User Manual FINE/Turbo v8," NUMECA International, Brussels, 2007.

[13] Yang, Z., and Shih, T. H., "A A-ϵ Model for Turbulence and Transitional Boundary Layer," *Near-Wall Turbulent Flows*, Elsevier, New York, 1993, pp. 165–175.

[14] Hirsch, C., and Tartinville, B., "RANS Modelling for Industrial Applications and Some Challenging Issues," *International Journal of Computational Fluid Dynamics*, Vol. 23, No. 4, 2009, pp. 295–303. doi:10.1080/10618560902773379

[15] Delery, J., "Turbulent Shock-Boundary Layer Interaction and Its Control," *Progress in Aerospace Sciences*, Vol. 22, No. 4, 1985, pp. 209–280. doi:10.1016/0376-0421(85)90001-6

[16] Atkin, C. J., and Squire, L. C., "A Study of the Interaction of a Normal Shock Wave with a Turbulent Boundary Layer at Mach Numbers Between 1.30 and 1.55," *European Journal of Mechanics, B/Fluids*, Vol. 11, No. 1, 1992, pp. 93–118.

[17] Doerffer, P., "An Experimental Investigation of the Mach Number Effect upon a Normal Shock Wave – Turbulent Boundary Layer Interaction on a Curved Wall," *Acta Mechanica*, Vol. 76, 1989, pp. 35–51.

P. Tucker
Associate Editor